Application of the Artificial Compression Method to the Simulation of Two-Dimensional Frontogenesis

Yang Hongwei (杨宏伟)[1], Wang Bin (王 斌), and Ji Zhongzhen (季仲贞)

LASG, Institute of Atmospheric Physics, Chinese Academy of Sciences, Beijing 100029

(Received September 9, 2001; revised June 24, 2002)

ABSTRACT

The artificial compression method (ACM) that is generally used to capture the contact discontinuity in nonviscous flows is used here in the simulation of quasi-geostrophic ideal frontogenesis in two dimensions. A comparison is made among the result of the ACM, the simulation result of Cullen, and the exact solution of the semi-geostrophic equations. The simulated front in this paper is more prominent than Cullen's and is much closer to the exact solution.

Key words: artificial compression method, frontogenesis, quasi-geostrophic, semi-geostrophic

1. Introduction

The frontogenesis area of China is mainly distributed from the south of China to the Changjiang drainage area and from the corridor on the west of the Huanghe River to the northeast of China. These are usually called south frontogenesis belt and the north frontogenesis belt, respectively. Especially in winter (summer), the forming of a front is usually a hint of snow disaster (rainstorm) in the north (south). So, for economic reasons in particular, it is important to forecast exactly when and where a front will form.

Mathematically, discontinuities exist in many strong weather phenomena. For example, a front in three dimensions can be considered approximately as a density discontinuity. Typhoons and squall lines can also be discribed this way. The discontinuity commonly transmits at the velocity of sound in an adiabatic gas, according to the theory of fluid mechanics. But if it transmits at the velocity of a gas, the discontinuity must be composed of the same particles along the transmission. The discontinuity is called the material interface or the contact discontinuity. Although a front in the atmosphere is not a rigorous contact discontinuity, the velocity of the front is similar to the velocity of a contact discontinuity in fluid mechanics. In order to keep the theory simple, the front is commonly assumed as a contact discontinuity. And on this point, researchers have obtained some results that coincide with observation.

From the view of conservation laws in Euler coordinates, the characteristics on both sides of a shock contract to the shock itself, and the computing error does not smooth the shock. Unlike the shock however, the difficulty in successfully simulating a contact discontinuity is that the characteristics on both sides of a contact discontinuity are almost parallel. Unless there is additional modification, the computing error at the discontinuity will make the contact discontinuity spread and smooth. So, when computing frontogenesis with

[1]E-mail: hyang@lasg.iap.ac.cn

common finite difference schemes, the width is increased and the boundaries become more and more ambiguous with the passing of time.

Hoskins (1982) reviewed many works on frontogenesis theories and deduced the following equations through a deformation field (Hoskins and Bretherton 1972).

$$u_t + uu_x + wu_z + \varphi_x - fv = 0 \ , \tag{1}$$

$$v_t + uv_x + \alpha v + wv_z + f(\alpha x + u) = 0 \ , \tag{2}$$

$$\theta_t + u\theta_x + w\theta_z = 0 \ , \tag{3}$$

$$u_x + \alpha + w_z = 0 \ , \tag{4}$$

$$\varphi_z = g\frac{\theta}{\theta_0} \ . \tag{5}$$

In these quasi-geostrophic equations, u, v, w, and θ form the front in the special trend. This front appears first at the upper and lower boundaries, then develops into the interior of the fluid at low speed. This point coincides with observation. For instance, the folding of the tropopause implies the forming of a front discontinuity. In fact, the nonviscous quasi-geostrophic equations have Kelvin-Helmholz and turbulent instabilities. So, viscosity is added to the equations in practical computing (Blumen 1990; Vallis 1992). The result of the artificial compression method (ACM) (Jin 1993) and the simulation result of Cullen (1983; 1984) are compared in this paper and the former is closer to the exact solution of the semi-geostrophic equations.

2. Artificial compression method

The scheme used in this paper is the hybrid scheme developed by Jin (1993) with ACM for solving the Euler equations. The scheme is introduced as a scalar equation in one dimension. Assume the equation as

$$\frac{\partial u(x,t)}{\partial t} + \frac{\partial f[u(x,t)]}{\partial x} = 0 \ .$$

The grids are uniform in space, the step is Δx, $x_j = j\Delta x$, and the time step is Δt, $t^n = n\Delta t$. The scheme is a conservation form scheme, denote $u(x_j, t^n)$ by u_j^n then the scheme of Jin (1993) is given by

$$u_j^{n+1} = u_j^n - \lambda(\hat{f}^n_{j+\frac{1}{2}} - \hat{f}^n_{j-\frac{1}{2}}) \ , \tag{6}$$

where $\lambda \equiv \Delta t / \Delta x$, $f_i^n \equiv f(u_j^n)$, and $\Delta u^n_{j+\frac{1}{2}} \equiv u^n_{j+1} - u^n_j$. The numerical flux $\hat{f}^n_{j+\frac{1}{2}}$ is given by

$$\hat{f}^n_{j+\frac{1}{2}} = \begin{cases} f^{HRS}_{j+\frac{1}{2}}, & \left|\Delta u^n_{j+\frac{1}{2}}\right| > \max(\varepsilon\Delta x, 0\min(\left|\Delta u^n_{j-\frac{1}{2}}\right|, \left|\Delta u^n_{j+\frac{3}{2}}\right|)) \\ f^{LW}_{j+\frac{1}{2}} \ , & \text{otherwise} \ , \end{cases}$$

where $f^{LW}_{j+\frac{1}{2}}$ is the numerical flux of the Lax-Wendroff Scheme and $f^{HRS}_{j+\frac{1}{2}}$ is the numerical flux of the high resolution scheme of the following modified equation

$$\frac{\partial u(x,t)}{\partial t} + \frac{\partial}{\partial x}[au + L(u)] = 0 \ . \tag{7}$$

Let

$$f^{HRS}_{j+\frac{1}{2}} = \frac{1}{2}[au^n_j + au^n_{j+1} + L^n_j + L^n_{j+1} + g^n_j + g^n_{j+1} - Q(a+\mu^{HRS}_{j+\frac{1}{2}} + \gamma^n_{j+\frac{1}{2}})\Delta u^n_{j+\frac{1}{2}}] ,$$

where

$$\mu^{HRS}_{j+\frac{1}{2}} = \begin{cases} (L^n_{j+1} - L^n_j)/\Delta u^n_{j+\frac{1}{2}} , & \Delta u^n_{j+\frac{1}{2}} \neq 0 , \\ 0 , & \Delta u^n_{j+\frac{1}{2}} = 0 , \end{cases}$$

$$\gamma^n_{j+\frac{1}{2}} = \begin{cases} (g^n_{j+1} - g^n_j)/\Delta u^n_{j+\frac{1}{2}} , & \Delta u^n_{j+\frac{1}{2}} \neq 0 , \\ 0 , & \Delta u^n_{j+\frac{1}{2}} = 0 , \end{cases}$$

$$g^n_j = M(\tilde{g}^n_{j-\frac{1}{2}}, \tilde{g}^n_{j+\frac{1}{2}}) , \quad \text{and}$$

$$\tilde{g}^n_{j+\frac{1}{2}} = \frac{1}{2}[Q(a+\mu^{HRS}_{j+\frac{1}{2}}) - \lambda(a+\mu^{HRS}_{j+\frac{1}{2}})^2]\Delta u^n_{j+\frac{1}{2}} ,$$

where $Q(x) = |x|$. Note that L^n_j has the following form

$$L^n_j = S \cdot \max[0, M(\alpha L^n_{j-\frac{1}{2}}, L^n_{j+\frac{1}{2}}) \cdot S, M(L^n_{j-\frac{1}{2}}, \alpha L^n_{j+\frac{1}{2}}) \cdot S] ,$$

where $S = \mathrm{sgn}(L^n_{j+\frac{1}{2}})$. And M and $L^n_{j+\frac{1}{2}}$ are given as

$$M(x, y) = \begin{cases} \mathrm{sgn}(x)\min(|x|, |y|) , & x \cdot y > 0 , \\ 0 , & x \cdot y < 0 , \end{cases}$$

$$L^n_{j+\frac{1}{2}} = \frac{1}{2}(Q(a) - \lambda a^2)[\Delta u^n_{j+\frac{1}{2}} - M(\Delta u^n_{j-\frac{1}{2}}, \Delta u^n_{j+\frac{1}{2}}, \Delta u^n_{j+\frac{3}{2}})] .$$

Here, α serves to judge the position of the discontinuity, and

$$\frac{1}{2}\alpha = \left| \frac{\left|\Delta u^n_{j+\frac{1}{2}}\right|^\beta - \left|\Delta u^n_{j-\frac{1}{2}}\right|^\beta}{\left|\Delta u^n_{j+\frac{1}{2}}\right|^\beta + \left|\Delta u^n_{j-\frac{1}{2}}\right|^\beta} \right| , \quad \beta = 2.5 ,$$

here $\beta = 2.5$ serves to make the discontinuity prominent.

3. Numerical simulation

Multiply Eq.(4) by u and add the result to Eq.(1), multiply Eq.(4) by v and add the result to Eq.(2), multiply Eq.(4) by θ and add the result to Eq.(3), denote $v + fx$ by M, then the primitive equations can be written as

$$u_t + (u^2)_x + (wu)_z = -\alpha u - \varphi_x + fv , \tag{8}$$

$$M_t + (uM)_x + (wM)_z = -2\alpha M , \tag{9}$$

$$\theta_t + (u\theta)_x + (w\theta)_z = -\alpha\theta , \tag{10}$$

$$u_x + \alpha + w_z = 0 , \tag{11}$$

$$\varphi_z = g\frac{\theta}{\theta_0} \tag{12}$$

The computing domain is a rectangular area with length $2L$ and height H. The initial conditions are

$$\begin{cases} u = -\alpha x \ , \\ M = fX \ , \\ \theta = \theta_0 + \theta_1 \tan^{-1}[5X(x, z)/L] \ , \end{cases} \tag{13}$$

where X is defined implicitly by the equation

$$[x - X(x, z)]/(z - H/2) = (-5g\theta_1/\theta_0 Lf^2)\{1 + [5X(x, z)/L]^2\}^{-1} \tag{14}$$

The boundary conditions at $x = \pm L$ are

$$\begin{cases} u = \mp \alpha L \ , \\ M = \pm fL \ , \\ \theta = \theta_0 \pm \theta_1 \tan^{-1}(5) \ . \end{cases} \tag{15}$$

and at $z = 0$, $z = H$, the boundary conditions are $w = 0$. The grid is shown in Fig. 1.

At the intersection of a dotted line and solid line (Fig. 1), a middle variable $w^*_{i,j+1/2}$ is defined, then the vertical boundary conditions are $w^*_{i,-1/2} = 0$ and $w^*_{i,J+1/2} = 0$. One can derive $w = 0$ at $t = 0$ from the initial and boundary conditions. The computing method is described with a model equation

$$\eta_t + f(\eta)_x + g(\eta)_z = s(\eta) + k_v \eta_{xx} \ .$$

The first step: solve the following equation by the second order Runge–Kutta method with a time step $\Delta t/2$,

$$\eta_t = s(\eta) + k_v \eta_{xx} \ .$$

The second step: solve the following equation by the hybrid scheme with a time step $\Delta t/2$,

$$\eta_t + f(\eta)_x = 0 \ .$$

In computing practice, $f^n_{i+1/2}$ is used as the numerical flux of the high resolution

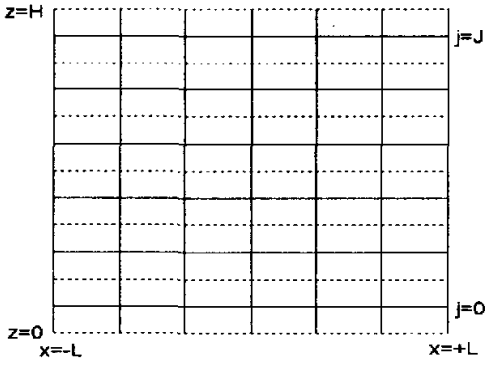

Fig. 1. Distribution of the grid.

scheme at these indexes k when $\Delta\theta''_{k+1/2}=\max\{\Delta\theta''_{i+1/2}, i=1,2,\cdots\}$, and the numerical flux of the Lax–Wendroff scheme is used at the other indexes.

The third step: solve the following equation by the hybrid scheme with a time step Δt,

$$\eta_t+g(\eta)_z=0\ .$$

The fourth step: repeat the second step.

The fifth step: repeat the first step.

Using the above five steps to solve the following equations,

$$M_t+(uM)_x+(wM)_z=-2\alpha M+k_v M_{xx}\ , \tag{16}$$

$$\theta_t+(u\theta)_x+(w\theta)_z=-\alpha\theta+k_v\theta_{xx}\ , \tag{17}$$

one can obtain M and θ at $t+\Delta t$ from M and θ at t. Because solving w^* from Eq.(4) is an overdetermined problem, we use the technique employed by Cullen (1983) to modify u so that Eq.(4) can be exactly satisfied in the discrete sense.

First, solve the following equation by the above five steps and denote the result by u^*,

$$u_t+(u^2)_x+(wu)_z=-\alpha u-(\varphi-\varphi^*)_x+fv+k_v u_{xx}\ , \tag{18}$$

where $\varphi=\varphi^*$ at $t=0$. The resulting value u^* will not satisfy Eq.(4), so we seek a function φ^* independent of z such that

$$u(t+\Delta t)=u^*(t+\Delta t)-\Delta t\delta_x\varphi^*(t)\ . \tag{19}$$

Therefore, from Eq.(4) we have

$$[u^*(t+\Delta t)-\Delta t\delta_x\varphi^*(t)]_x+\alpha+w_z^*=0\ . \tag{20}$$

Because of $w^*=0$ at $z=0$ and $z=H$, we make Eq.(20) discrete and sum them from $j=0$ to J to get

$$(J+1)\alpha+\sum_{j=0}^{J}\delta_x u_j^*(t+\Delta t)-(J+1)\Delta t\delta_x\delta_x\varphi^*(t)=w^*(H)-w^*(0)=0\ . \tag{21}$$

Let $u^*(\pm\alpha L)=u(\pm\alpha L)$, then $\varphi_x^*(\pm\alpha L)=0$. So we can solve φ^* from Eq.(21), $u(t+\Delta t)$ and $w^*(t+\Delta t)$ from Eq.(19) and Eq.(20). By the interpolation method we get $w(t+\Delta t)$ from $w^*(t+\Delta t)$. At last we solve $\varphi(t+\Delta t)$ from Eq.(5).

4. Results

The simulations were done using grids of 100×10, 200×20, and 200×40, where

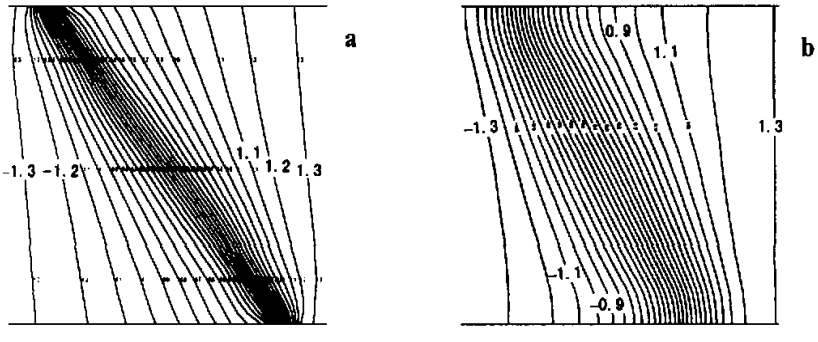

Fig. 2. (a) Potential temperature deviation at 13.9 h, 100×10, $k_v=8\times 10^4$ m^2 s^{-1}, (b) The simulation result of Cullen (1983).

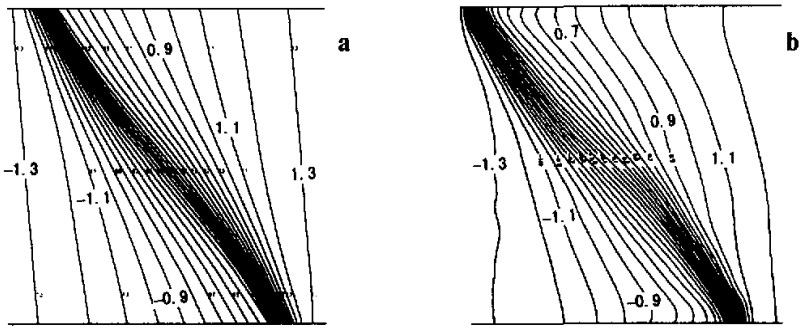

Fig. 3. (a) Potential temperature deviation at 13.9 h, 200 × 20, $k_c = 3 \times 10^4$ m^2 s^{-1}, (b) The simulation result of Cullen (1983).

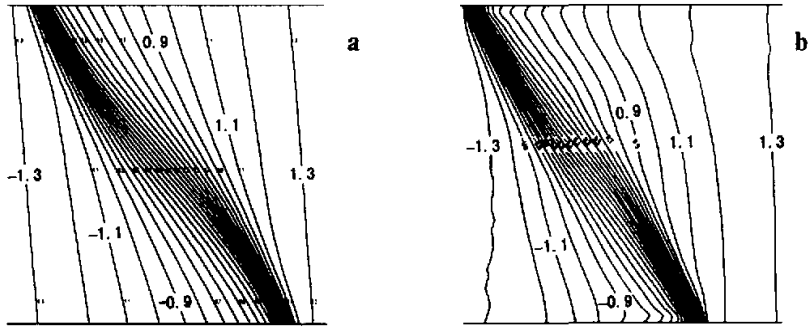

Fig. 4. (a) Potential temperature deviation at 13.9 h, 200 × 40, $k_1 = 2 \times 10^4$ m^2 s^{-1}, (b) The simulation result of Cullen (1983).

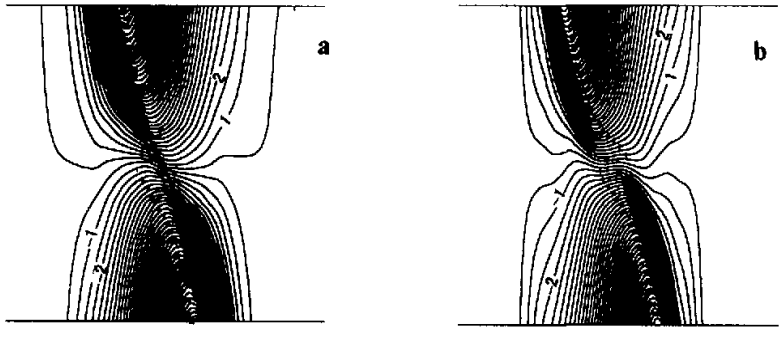

Fig. 5. Long-front wind at 13.9 h, 100 × 10, $k_1 = 3 \times 10^4$ m^2 s^{-1}.

Fig.6. Long-front wind at 13.9 h, 200 × 40, $k_1 = 2 \times 10^4$ m^2 s^{-1}.

$L=500$ km, $H=10$ km, $\theta_0=300$ K, $\theta_1=1$ K, Coriolis parameter $f=10^{-4}$ s^{-1}, and $\alpha=10^{-5}$. The comparison results are shown in Figs. 2–6.

5. Conclusions

In Euler coordinates, high resolution schemes for capturing shock wave have achieved great success. By modifying the primitive partial differential equations, researchers have made the contact discontinuity have some properties of a shock wave. Some high contact discontinuity resolution schemes have been developed on this point, such as the ACM of Harten (1977; 1978) and the ACM of Jin (1993), etc. We successfully simulate the ideal frontogenesis of the quasi-geostrophic equations in two dimensions in this paper. Even under the same coarse grid, the resolution obtained is higher than Cullen's, and the result in this paper is closer to the exact solution (Cullen 1983; Cullen and Purser 1984) than Cullen's.

Acknowledgments. The project was supported by the National Key Planning Development Project for Basic Research (G1999032801) and the Key Innovation Project of the Chinese Academy of Sciences (KZCX2-208).

REFERENCES

Blumen, W., 1990: A semigeostrophic Eady-Wave frontal model incorporating momentum diffusion, Part I: Model and solution. *J. Atmos. Sci.*, **47**, 1890–2902.

Cullen, M. J. P., 1983: Solutions to a model of a front forced by deformation. *Quart. J. Roy. Meteor. Soc.*, **109**, 565–573.

Cullen, M. J. P., 1984: Solutions of some nonlinear partial differential equations relevant to meteorology and implications for numerical methods. *Numerical Methods for Weather Prediction*, **1**, 225–253.

Cullen, M. J. P., and R. J. Purser, 1984: An extended Lagrangian theory of semigeostrophic frontogenesis. *J. Atmos. Sci.*, **41**, 1477–1497.

Jin Baoxia, 1993: An artificial compression method for the computation of contact discontinuities. *Journal of Computational Mathematics*, **1**, 121–128 (in Chinese).

Hoskins, B. J., 1982: The mathematical theory of frontogenesis. *Ann. Rev. Fluid Mech.*, **14**, 131–151.

Hoskins, B. J., and F. P. Bretherton, 1972: Atmospheric frontogenesis models: mathematical formulation and solution. *J. Atmos. Sci.*, **29**, 11–37.

Harten, A., 1977: The artificial compression method for computation of shocks and contact discontinuities, I. Single conservation laws. *Communications on Pure and Applied Mathematics*, **xxx**, 611–638.

Harten, A., 1978: The artificial compression method for computation of shocks and contact discontinuities, III. Self-adjusting hybrid schemes. *Mathematics of Computation*, **32**, 363–389.

Vallis, G. K., 1992: Mechanisms and parameterizations of geostrophic adjustment and a variational approach to balanced flow. *J. Atmos. Sci.*, **49**, 1144–1160.

反扩散格式在二维锋生数值模拟中的应用

杨宏伟　王　斌　季仲贞

摘　要

把无粘流中能成功捕捉接触间断的反扩散差分格式，用在了准地转二维理想锋生的数值模拟中，并将计算结果与 Cullen 的计算结果和半地转方程的精确解进行了比较。用反扩散格式模拟的锋面较 Cullen 的结果更加显著，而且更接近半地转方程的精确解。

关键词：反扩散方法，锋生，准地转，半地转